JOURNAL OF GUIDANCE, CONTROL, AND DYNAMICS
Vol. 29, No. 6, November–December 2006

Engineering Notes

ENGINEERING NOTES are short manuscripts describing new developments or important results of a preliminary nature. These Notes should not exceed 2500 words (where a figure or table counts as 200 words). Following informal review by the Editors, they may be published within a few months of the date of receipt. Style requirements are the same as for regular contributions (see inside back cover).

Flight Test of Model-Matching Controller for In-Flight Simulator MuPAL-α

Masayuki Sato*
Japan Aerospace Exploration Agency, Tokyo 181-0015, Japan

DOI: 10.2514/1.25685

Nomenclature

$\{A, B, C, D\}$	=	state-space representation of a system with transfer function $D + C(sI - A)^{-1}B$
$G(s)$	=	transfer function of system G
$\|G(s)\|_\infty$	=	H_∞ norm of system G
$\boldsymbol{I}$	=	appropriately dimensioned identity matrix
p	=	roll rate
q	=	pitch rate
r	=	yaw rate
u	=	forward–backward velocity
v	=	side velocity
w	=	vertical velocity
δ_a, δ_{a_c}	=	aileron deflection (rad) and command (rad)
δ_{DLC}, δ_{DLC_c}	=	direct lift control (DLC) flap deflection (rad) and command [rad]
δ_e, δ_{e_c}	=	elevator deflection (rad) and command (rad)
δ_{pl}, δ_{pl_c}	=	power lever deflection (mm) and command (mm)
δ_r, δ_{r_c}	=	rudder deflection (rad) and command (rad)
θ	=	pitch angle
τ	=	engine torque
ϕ	=	roll angle
ψ	=	yaw angle
$\mathbf{0}$	=	appropriately dimensioned zero matrix

I. Introduction

THE Japan Aerospace Exploration Agency (JAXA) has been developing a new in-flight simulator, the multipurpose aviation laboratory-α (MuPAL-α) [1] (Fig. 1), and a flight controller to enable it to simulate the motions of different aircraft. A model-matching or model-following controller is to be used for this purpose, similarly to other in-flight simulators such as the total in-flight simulator (TIFS) [2], the variable stability and response airplane (VSRA) [3,4], the advanced technologies testing aircraft system (ATTAS) [5], and the variable stability in-flight simulator test aircraft (VISTA) [6]. Investigation into handling qualities is to be a primary research application for MuPAL, and so the objective of our flight controller design is to obtain a single controller which can simulate the maneuverability of a variety of target aircraft. Although the simulation of gust response is also important, pilots usually compensate for gusts immediately, that is, motions induced by gusts are immediately cancelled by the pilot, and so gust response simulation is less of a priority than the simulation of maneuverability. For this reason, we ignore the simulation of gust response in exchange for being able to simulate a wide variety of maneuverability.

One methodology to satisfy such a requirement is to design a model-matching controller using only a feedforward controller; that is, as shown in Fig. 2, design a right inverse system of the plant, which represents the dynamical model of MuPAL-α, as a "feedforward controller," and set the dynamical model of the aircraft to be simulated as the "model." With this framework, we can realize a variety of different maneuverability characteristics by simply exchanging models because, since the feedforward controller is a right inverse system of the "plant," the feedforward controller produces the "plant inputs" which are needed for the plant to produce the "model outputs."

Ideal inverse systems for continuous-time systems were first proposed by Silverman [7], but the design method proposed therein requires differentiators, which makes it impractical because it is impossible to create differentiators in real systems. To overcome this drawback, filtered-type inverse systems have been proposed by Yoshikawa and Sugie [8], and several design methods for them and some similar filtered-type inverse systems have been proposed (see Sato [9] and references therein). In our design, we adopt the definition of inverse systems presented in Sato [9] and the design method therein, because the inverse system presented in [9] encompasses the inverse system in [8]; other design methods usually produce right inverse systems with direct terms, which lead to high gain in the high frequency range that consequently makes them impractical to implement. An alternative approach is to extend the method of Yang [10] to the inverse system design, but this requires another system acting as a low-pass filter, which increases the degree of the inverse system and consequently leads to the increase of computational complexity for the on-board computers. For these reasons, we apply the design method of [9] to the design of the model-matching controller for MuPAL-α.

The most important contribution of this paper is that we demonstrate that the right inverse systems can simulate the maneuverability of a variety of target aircraft simply by replacing the dynamical model which represents the maneuverability of the target aircraft, and this has been confirmed by flight tests.

In the following, we first introduce the definition and design method of right inverse systems presented in [9], and then show our design for the linearized longitudinal and lateral-directional motions of MuPAL-α around some equilibrium point. MuPAL-α has two conventional inputs for lateral-directional motions (ailerons and rudder), and for longitudinal motions has two conventional inputs (elevator and propeller thrust) and an additional input, a direct lift control (DLC) flap. Therefore, MuPAL-α can simulate two variables for lateral-directional motions and three for longitudinal motions, and these are set as v and ϕ, and u, w, and θ, respectively. We then show flight test results which confirm that the designed right inverse systems have good model-matching performance with two models, and finally present conclusions.

Presented as Paper 379 at the 42nd AIAA Aerospace Sciences Meeting and Exhibit, Reno, Nevada, 5–8 January 2004; received 6 June 2006; revision received 12 July 2006; accepted for publication 12 July 2006. Copyright © 2006 by the American Institute of Aeronautics and Astronautics, Inc. All rights reserved. Copies of this paper may be made for personal or internal use, on condition that the copier pay the $10.00 per-copy fee to the Copyright Clearance Center, Inc., 222 Rosewood Drive, Danvers, MA 01923; include the code $10.00 in correspondence with the CCC.

*Researcher, Institute of Space Technology and Aeronautics, 6-13-1 Osawa, Mitaka, Tokyo 181-0015, Japan; sato.masayuki@jaxa.jp.

Fig. 1 Multipurpose aviation laboratory-α (MuPAL-α).

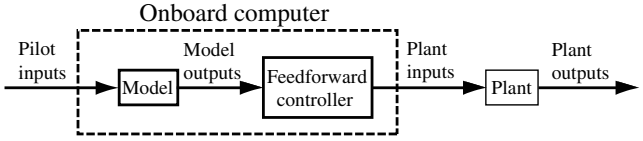

Fig. 2 Block diagram of model-matching controller using feedforward controller.

II. Controller Design

In this section, we describe the design method of the right inverse systems for linear time-invariant systems proposed in [9] and then apply it to the controller design for MuPAL-α.

A. Design Method of Right Inverse Systems

For completeness, we first show the definition of inverse systems introduced in [9].

Definition 1: Given a stable plant G and a stable diagonal weight function W, if there exists a stable and proper system $\bar{G}$ that satisfies (1), then $\bar{G}$ is a right inverse system of (G, W):

$$\|W(s)\{G(s)\bar{G}(s) - \boldsymbol{I}\}\|_\infty < 1 \tag{1}$$

If $\bar{G}$ satisfies this definition, then the cascaded system $Q = G\bar{G}$ satisfies the following Lemma, where the ith diagonal element of $W(s)$ is denoted as $W_i(s)$.

Lemma 1: If $\bar{G}$ satisfies the condition of Definition 1, then $Q = G\bar{G}$ satisfies (2–4), for any frequency ω_0 where $\zeta(\omega_0) := \min_i |W_i(j\omega_0)| > 1$ is satisfied:

$$1 - 1/\zeta(\omega_0) < |Q_{ii}(j\omega_0)| < 1 + 1/\zeta(\omega_0), \quad \forall\ i \tag{2}$$

$$|\angle Q_{ii}(j\omega_0)| < \arcsin 1/\zeta(\omega_0), \quad \forall\ i \tag{3}$$

$$|Q_{ij}(j\omega_0)| < 1/\zeta(\omega_0), \quad \forall\ i, j, \qquad i \neq j \tag{4}$$

where $Q_{ij}(j\omega_0)$ denotes element (i, j) of $Q(j\omega_0)$.

For the proof, please refer to [9].

Lemma 1 shows that if the minimum gain of W at some frequency is sufficiently large, then diagonal elements have almost unity gains and sufficiently small phase deviations from zeros, and nondiagonal elements have sufficiently small gains at the frequency. Although we have no descriptions on the phases of nondiagonal elements, the third inequality (4) shows that if the minimum gain of W at some frequency is sufficiently large, then the gains of nondiagonal elements at the frequency are all sufficiently small, and so the effects of phases are negligible. Therefore, Lemma 1 shows that $\bar{G}$ works as a right inverse system of G for any frequency where the minimum gain of W is sufficiently large.

The assumption of the stability of G seems to be a little restrictive at first, but we can easily satisfy it by first designing a feedback controller that stabilizes G, then designing $\bar{G}$ for the augmented system that includes the feedback controller. Thus, the stability assumption of G is not restrictive in practice.

From Definition 1, to design the right inverse system $\bar{G}$ is to solve the H_∞ control problem for the following generalized plant, where the state-space representations of G and W are, respectively, given as $\{A_p, B_p, C_p, D_p\}$ and $\{A_w, B_w, C_w, D_w\}$,

$$\begin{bmatrix} A & B_1 & B_2 \\ C_1 & D_{11} & D_{12} \\ C_2 & D_{21} & D_{22} \end{bmatrix} = \begin{bmatrix} A_p & \boldsymbol{0} & \boldsymbol{0} & B_p \\ B_w C_p & A_w & -B_w & B_w D_p \\ D_w C_p & C_w & -D_w & D_w D_p \\ \boldsymbol{0} & \boldsymbol{0} & \boldsymbol{I} & \boldsymbol{0} \end{bmatrix} \tag{5}$$

We assume that the right inverse system is full order, that is, that the degree of $\bar{G}$ is equal to the sum of the degrees of A_p and A_w, and if it has no direct term, then it is easily obtained as follows [11]:

$$\left\{\left(-P_g^{-1}L + B_2 W_f + AP_f\right)S^{-1}, -P_g^{-1}W_g, W_f S^{-1}, \boldsymbol{0}\right\} \tag{6}$$

where $S = P_f - P_g^{-1}$, after solving the following two linear matrix inequalities (LMIs) with the aid of software such as the LMI control toolbox [12]:

$$\begin{bmatrix} P_f & \boldsymbol{I} \\ \boldsymbol{I} & P_g \end{bmatrix} > 0 \tag{7}$$

$$\begin{bmatrix} Q_f & L^T + A & Q_{31}^T & B_1 \\ L + A^T & Q_g & C_1^T & Q_{24} \\ Q_{31} & C_1 & -\boldsymbol{I} & D_{11} \\ B_1^T & Q_{24}^T & D_{11}^T & -\boldsymbol{I} \end{bmatrix} < 0 \tag{8}$$

where $P_f = P_f^T, P_g = P_g^T, L, W_f$, and W_g are decision variables, and $Q_f = AP_f + P_f A^T + B_2 W_f + W_f^T B_2^T$, $Q_{31} = C_1 P_f + D_{12} W_f$, $Q_g = P_g A + A^T P_g$, and $Q_{24} = P_g B_1 + W_g$.

B. Controllers for MuPAL-α

We now design right inverse systems for the linearized longitudinal and lateral-directional motions of MuPAL-α at a true air speed of TAS = 66.5 m/s and an altitude of $H = 1520$ m.

The MuPAL-α actuators are modeled as follows:

$$\delta_e = \frac{1}{0.1s + 1}\delta_{e_c} \qquad \delta_{\mathrm{DLC}} = \frac{0.92}{0.07s + 1}\delta_{\mathrm{DLC}_c}$$
$$\delta_{\mathrm{pl}} = \frac{1}{0.08s + 1}\delta_{\mathrm{pl}_c} \tag{9}$$

$$\delta_a = \frac{1}{0.1s + 1}\delta_{a_c} \qquad \delta_r = \frac{1}{0.1s + 1}\delta_{r_c} \tag{10}$$

We, respectively, implement the following feedback controllers for the longitudinal and lateral-directional motions to lessen initial trim errors at the beginning of in-flight simulation experiments. Further, the controller (12) stabilizes the lateral-directional motions of MuPAL-α with actuator models in (10),

$$\delta_{e_c} = 0.3\theta \tag{11}$$

$$\delta_{a_c} = 0.2\phi \tag{12}$$

The plant systems Gs for which we want to design inverse systems are given as the augmented systems which are composed of the linearized longitudinal motions of MuPAL-α, (9) and (11), or the linearized lateral-directional motions of MuPAL-α, (10) and (12). Their state-space representations are, respectively, given in (A1) and (A2) in the Appendix.

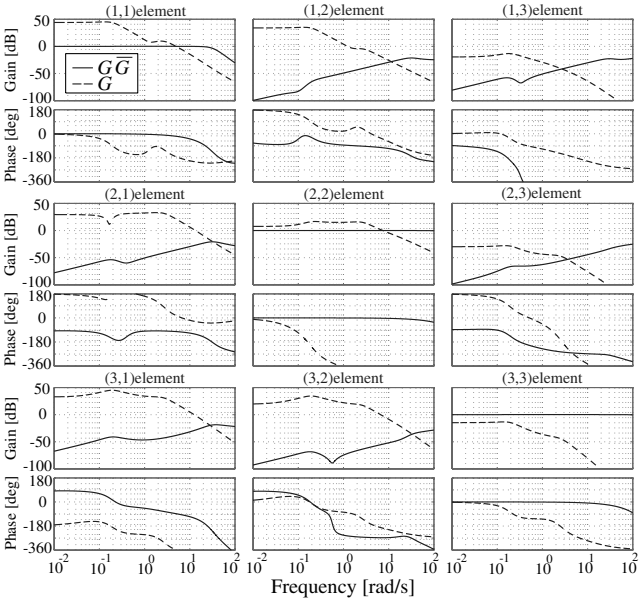

Fig. 3 Bode plots of the cascaded system Q for longitudinal motions.

The weight functions Ws that specify the performance of the $\bar{G}$s and their frequency ranges are, respectively, set as follows for longitudinal and lateral-directional motions:

$$W(s) = \frac{0.01s + 15}{s + 0.0015} I_3 \tag{13}$$

$$W(s) = \frac{0.01s + 15}{s + 0.0015} I_2 \tag{14}$$

These weight functions are set to satisfy the following design specification for the cascaded system $Q = G\bar{G}$, where G denotes the augmented system of longitudinal or lateral-directional motions, and $\bar{G}$ denotes the right inverse system to be designed.

1) For the low frequencies under 2 rad/s:

i) gain errors of diagonal elements of Q from unities must be less than 15%,

ii) delay times that are calculated as pure delay time from phase delays of diagonal elements of Q must be less than 15% of each cycle time, and

iii) gains of nondiagonal elements of Q must be less than 15%.

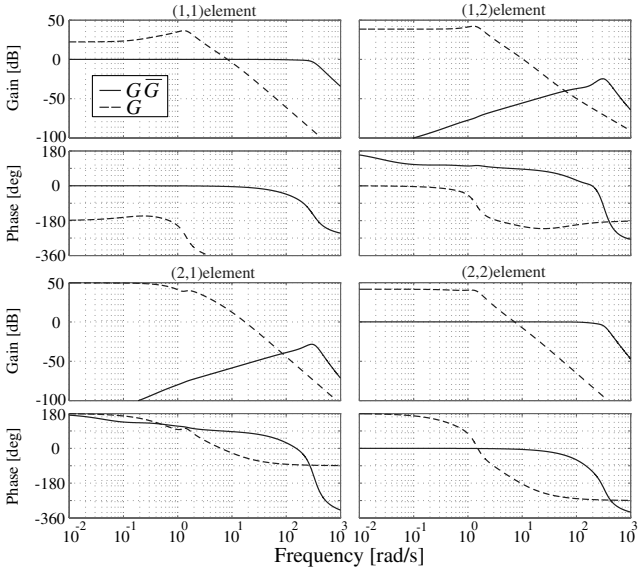

Fig. 4 Bode plots of the cascaded system Q for lateral-directional motions.

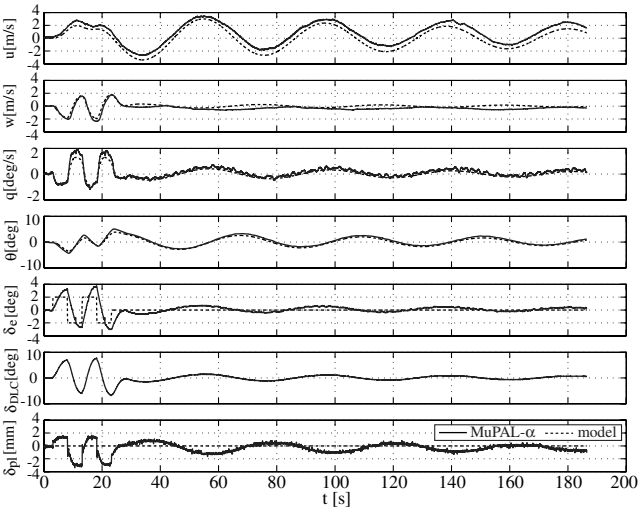

Fig. 5 Elevator doublet responses: B747 model.

In other words, $1/\zeta(\omega)$ in Lemma 1 is set as 0.15 for $\omega \in [0; 2]$. This design specification is given by considering that the periods of short-period mode and dutch-roll mode of civil aircraft are almost greater than 3 s, that is, their oscillation frequencies are almost less than about 2 rad/s. Therefore, the above design specification is adequate for the model-matching controller design for MuPAL-α. However, if we need to simulate military aircraft motions, the above design specification may be inadequate. The relationships among the designed controller performance, the preciseness of plant models, and the weight functions were investigated in the conference version of this paper [11]; for further details on setting the weight functions (13) and (14), please refer to it.

After solving LMIs (7) and (8) for longitudinal and lateral-directional motions, we obtain right inverse systems for each motion. Their degrees are, respectively, 11 and 8 for longitudinal and lateral-directional motions. We omit their state-space representations due to lack of space. Figures 3 and 4, respectively, show the Bode plots of Qs for longitudinal and lateral-directional motions. The Bode plots of Gs are also drawn for comparison. We easily confirm that, not only for low frequencies under 2 rad/s but also for the middle frequencies from 2 to 10 rad/s, the diagonal elements of Qs have almost unity gains and have very small phase delays, and the nondiagonal elements of Qs have very small gains. Although the nondiagonal elements of Qs have large phase deviations from zeros, their effects are negligibly small because they have very small gains for low frequencies under 2 rad/s. Therefore, the designed $\bar{G}$s are confirmed to work as the right inverse systems of each plant for low frequencies under 2 rad/s.

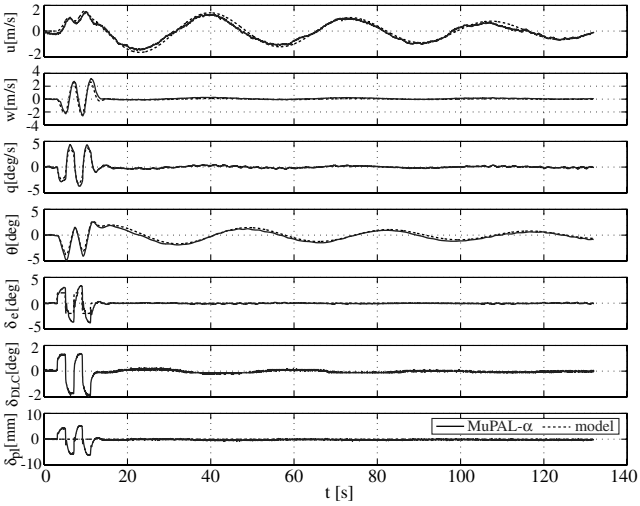

Fig. 6 Elevator doublet responses: Jet Star model.

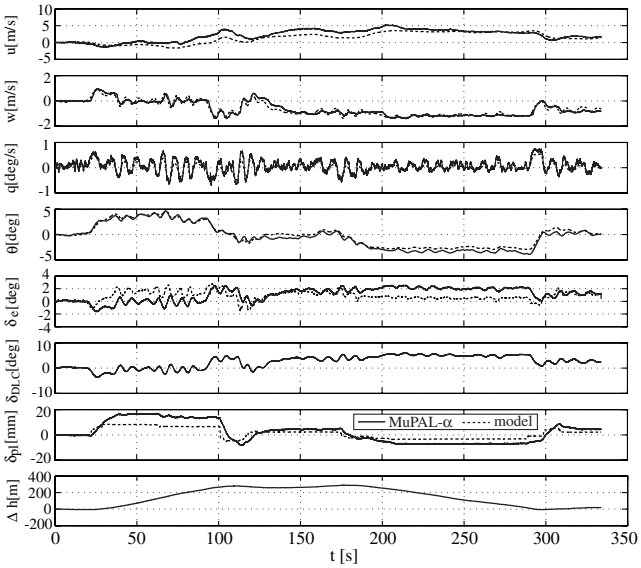

Fig. 7 Time history of climb and descent: B747 model.

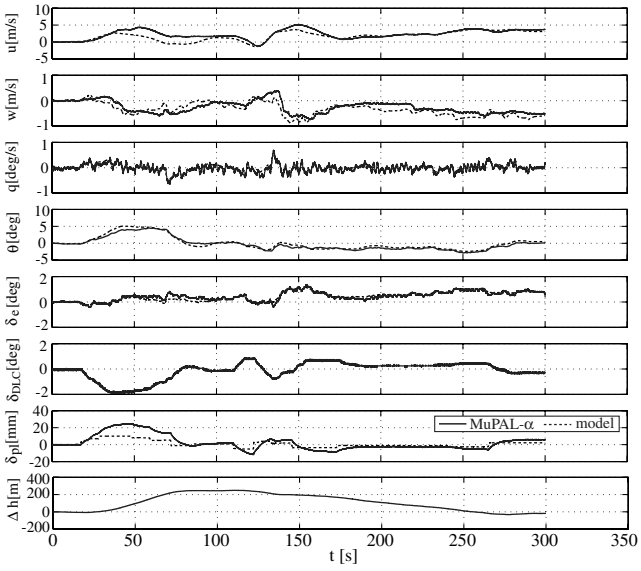

Fig. 8 Time history of climb and descent: Jet Star model.

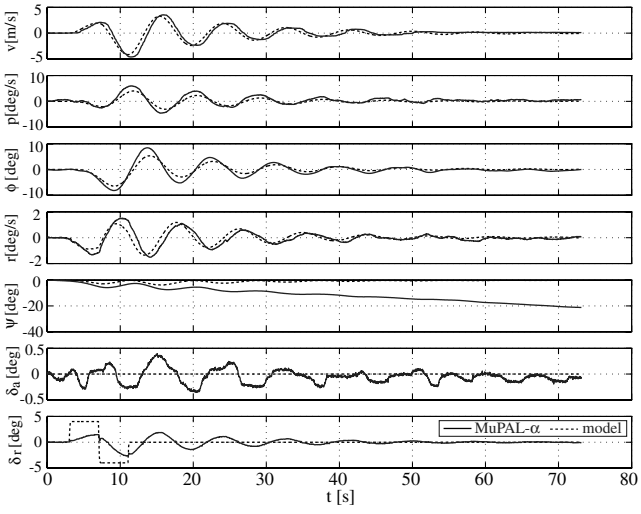

Fig. 9 Rudder doublet responses: B747 model.

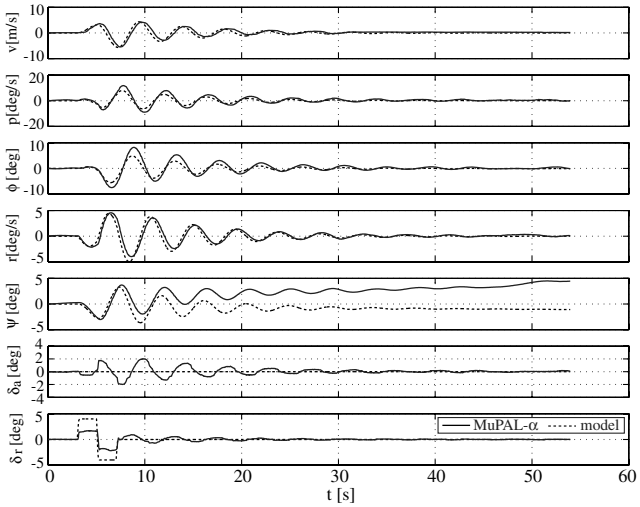

Fig. 10 Rudder doublet responses: Jet Star model.

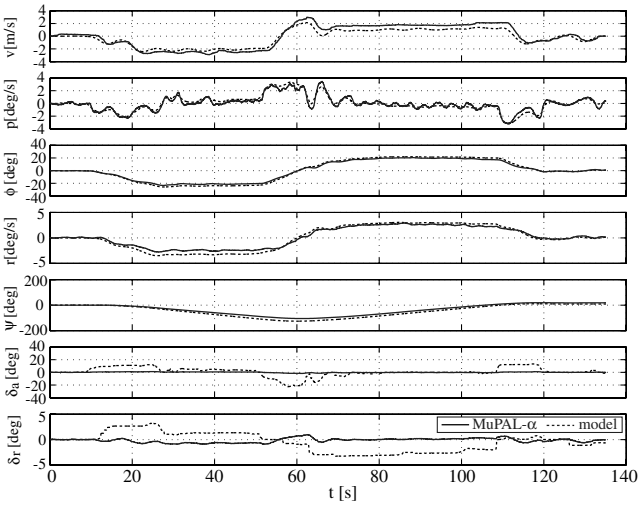

Fig. 11 Time history of turns: B747 model.

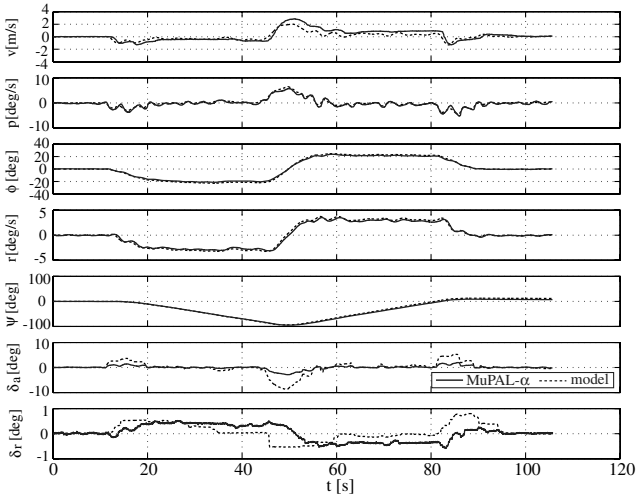

Fig. 12 Time history of turns: Jet Star model.

III. Flight Tests

We use two aircraft models to verify the performance of the designed right inverse systems: a Boeing 747 [13] and a Lockheed Jet Star [13]. Engine data for these models were not available, so the aircraft engines are both modeled as a first-order system with a time constant of 5 s.

We implement right inverse systems after discretizing them using bilinear transformation with 0.02 s. We also implement a filter $1/(0.03s + 1)^3$ for each pilot input after discretizing it using zero-order hold with 0.02 s to reduce electrical noise. The models are implemented after discretization using a zero-order hold with 0.02 s.

We first verified the performance of the right inverse systems by hardware-in-the-loop (HIL) simulations, which confirmed that they worked as the right inverse systems of each augmented system; that is, they exhibited a good model-matching performance for the two models. (Time histories are omitted for lack of space.) After HIL simulations, we conducted flight tests to verify their performance under real conditions.

In flight tests, encountering gusts is inevitable, and under the influence of gusts the variables to be matched will exhibit discrepancies with the model data because the model-matching controller has neither servo nor regulator functions. For this reason, we conducted the following flight tests under as calm conditions as possible. However, even if MuPAL-α encounters severe gusts the realization of maneuverability which is shown in the following holds because the simulation of maneuverability is realized with only feedforward controllers. (In such a case, variables to be matched will have wide discrepancies with the model's data in time history data; however, the maneuverability is realized.)

Figures 5 and 6 show the models' responses to elevator doublets, and Figs. 7 and 8 show time histories of climb and descent under manual pilot control, where Δh denotes the height deviation of MuPAL-α. These tests were executed under conditions differing slightly from the nominal: TAS = 65–73 m/s and H = 2000–2500 m/s. Although the forward–backward velocity u of MuPAL-α in Figs. 7 and 8 sometimes shows discrepancies with the model data, other variables to be matched, w and θ in Figs. 5–8 and u in Figs. 5 and 6, correspond closely with the model data; that is, MuPAL-α faithfully simulates the longitudinal maneuverability of the target aircraft.

Figures 9 and 10 show the models' responses to a rudder doublet, and Figs. 11 and 12 show time histories of turns under manual pilot control. These tests were executed under conditions differing slightly from the nominal: TAS = 65–69 m/s and H = 1800–2100 m/s. We did not implement any yaw stability augmentation systems for the B747 model; therefore the oscillation frequency and the damping ratio of the dutch-roll mode are very low, and thus it took a long time for the dutch-roll mode to be settled. Although roll angle ϕ in Figs. 9 and 10 shows discrepancies with the model data, other variables to be matched, v in Figs. 9–12 and ϕ in Figs. 11 and 12, correspond closely with the model data; that is, MuPAL-α faithfully simulates the lateral-directional maneuverability of the target aircraft.

In these tests, we did not change the model-matching controller of MuPAL-α, but simply replaced the model in Fig. 2; that is, our designed controller is confirmed to realize a variety of maneuverability simply by replacing models.

IV. Conclusions

We present the model-matching controller design for an in-flight simulator MuPAL-α for its linearized longitudinal and lateral-directional motions around an equilibrium point and show flight test results of designed controllers. The controllers are composed of simple feedback controllers, which are designed to reduce initial trim errors, and feedforward controllers which are right inverse systems of linearized longitudinal or lateral-directional motions of MuPAL-α with each actuator model and each simple feedback controller. In this framework, we ignore the simulation of aircraft motions due to gusts, which is the only drawback of our design; however, we attain a large range of maneuverability simply by replacing the models which represent the dynamic models of target aircraft, and this has been confirmed by flight tests.

Appendix: State-Space Representations of Linearized Motions of MuPAL-α with Actuator Models and Feedback Controllers

$$\begin{bmatrix} A & B \\ C & D \end{bmatrix} = \begin{bmatrix} -0.016231 & 0.17214 & -6.0900 & -9.7638 & 0.026805 & 0.46601 & 0.36894 & 0 & 0 & 0 & 0 \\ -0.18323 & -1.0930 & 64.546 & -0.91532 & -5.9310 \times 10^{-3} & -4.9383 & -6.7070 & 0 & 0 & 0 & 0 \\ 7.9857 \times 10^{-3} & -0.069232 & -1.9025 & 6.6727 \times 10^{-3} & 6.7679 \times 10^{-4} & -4.2540 & 0.83489 & 0 & 0 & 0 & 0 \\ 0 & 0 & 1.0000 & 0 & 0 & 0 & 0 & 0 & 0 & 0 & 0 \\ 0 & 0 & 0 & 0 & -2.2133 & 0 & 0 & 3.1267 & 0 & 0 & 0 \\ 0 & 0 & 0 & 3.0000 & 0 & -10.000 & 0 & 0 & 10.000 & 0 & 0 \\ 0 & 0 & 0 & 0 & 0 & 0 & -14.286 & 0 & 0 & 13.143 & 0 \\ 0 & 0 & 0 & 0 & 0 & 0 & 0 & -12.500 & 0 & 0 & 12.500 \\ 1 & 0 & 0 & 0 & 0 & 0 & 0 & 0 & 0 & 0 & 0 \\ 0 & 1 & 0 & 0 & 0 & 0 & 0 & 0 & 0 & 0 & 0 \\ 0 & 0 & 0 & 57.296 & 0 & 0 & 0 & 0 & 0 & 0 & 0 \end{bmatrix} \tag{A1}$$

where the state variables are $[u$ (m/s), w (m/s), q (rad/s), θ (rad), τ (%), δ_e (rad), δ_{DLC} (rad), and δ_{pl}(mm)$]^T$; the input variables are $[\delta_{e_c}$ (rad), δ_{DLC_c} (rad), and δ_{pl_c} (mm)$]^T$; and the output variables are $[u$ (m/s), w (m/s), and θ (deg)$]^T$.

$$\begin{bmatrix} A & B \\ C & D \end{bmatrix} = \begin{bmatrix} -0.17810 & 6.0791 & 9.7633 & -65.623 & 0 & 2.8900 & 0 & 0 \\ -0.057500 & -3.8100 & 0 & 1.3430 & -10.750 & 1.1870 & 0 & 0 \\ 0 & 1.0000 & 0 & 0.094352 & 0 & 0 & 0 & 0 \\ 0.025300 & -0.062800 & 0 & -0.47500 & 0.34500 & -2.2200 & 0 & 0 \\ 0 & 0 & 2.0000 & 0 & -10.000 & 0 & 10.000 & 0 \\ 0 & 0 & 0 & 0 & 0 & -10.000 & 0 & 10.000 \\ 1 & 0 & 0 & 0 & 0 & 0 & 0 & 0 \\ 0 & 0 & 57.296 & 0 & 0 & 0 & 0 & 0 \end{bmatrix} \tag{A2}$$

where the state variables are [v (m/s), p (rad/s), ϕ (rad), r (rad/s), δ_a (rad), and δ_r (rad)]^T; the input variables are [δ_{a_c} (rad), δ_{r_c} (rad)]^T; and the output variables are [v (m/s), ϕ (deg)]^T.

References

[1] Masui, K., and Tsukano, Y., "Development of a New In-Flight Simulator MuPAL-α," AIAA Paper 2000-4574, Aug. 2000.

[2] Motyka, P. R., Rynaski, E. G., and Reynolds, P. A., "Theory and Flight Verification of the TIFS Model-Following System," *Journal of Aircraft*, Vol. 9, No. 5, 1972, pp. 347–353.

[3] Kawahata, N., "Model-Following System with Assignable Error Dynamics and Its Application to Aircraft," *Journal of Guidance and Control*, Vol. 3, No. 6, 1980, pp. 508–516.

[4] Komoda, M., Kawahata, N., Tsukano, Y., and Ono, T., "VSRA In-Flight Simulator—Its Evaluation and Applications," AIAA Paper 88-4605-CP, Sept. 1988.

[5] Hanke, D., and Lange, H. H., "Flight Evaluation of the ATTAS Digital Fly-By-Wire/Light Flight Control System," *Proceedings of ICAS 16th Congress*, ICAS, Jerusalem, Israel, 1988, pp. 866–876.

[6] Weingarten, N. C., "History of In-Flight Simulation at General Dynamics," *Journal of Aircraft*, Vol. 42, No. 2, 2005, pp. 290–298.

[7] Silverman, L. M., "Inversion of Multivariable Linear Systems," *IEEE Transactions on Automatic Control*, Vol. 14, No. 3, 1969, pp. 270–276.

[8] Yoshikawa, T., and Sugie, T., "Filtered Inverse Systems," *International Journal of Control*, Vol. 43, No. 6, 1986, pp. 1661–1671.

[9] Sato, M., "Gain-Scheduled Inverse System and Filtering System Without Derivatives of Scheduling Parameters," *Proceedings of the American Control Conference*, IEEE, Denver, CO, 2003, pp. 4173–4178.

[10] Yang, C. D., Ouyang, J., and Ju, H. S., "Pilot Prefilter Design via H_∞ Model-Matching Approach," *Journal of Guidance, Control, and Dynamics*, Vol. 20, No. 1, 1997, pp. 186–189.

[11] Sato, M., "Model-Matching Controller Using Right Inverse System and Its Verification by Flight Experiments," AIAA Paper 2004-379, Jan. 2004.

[12] Gahinet, P., Nemirovski, A., Laub, A., and Chilali, M., "LMI Control Toolbox User's Guide," The Math Works Inc., Natick, MA, 1995.

[13] Heffley, R. K., and Jewell, W. F., "Aircraft Handling Qualities Data," NASA CR-2144, Washington, D.C., Dec. 1972.